

An experimental study of expanding spherical laminar lean H2/O2/N2/He flames

Downloaded from: https://research.chalmers.se, 2026-11-23 08:49 UTC

Citation for the original published paper (version of record):
Hsieh, H., Shy, S., Lipatnikov, A. (2027). An experimental study of expanding spherical laminar lean H2/O2/N2/He flames. Combustion and Flame, 295: 1-9.
http://dx.doi.org/10.1016/j.combustflame.2026.115441

N.B. When citing this work, cite the original published paper.

research.chalmers.se offers the possibility of retrieving research publications produced at Chalmers University of Technology. It covers all kind of research output: articles, dissertations, conference papers, reports etc. since 2004. research.chalmers.se is administrated and maintained by Chalmers Library

(article starts on next page)

Combustion and Flame 295 (2027) 115441

Contents lists available at ScienceDirect

Combustion and Flame

journal homepage: www.sciencedirect.com/journal/combustion-and-flame

An experimental study of expanding spherical laminar lean $H_2/O_2/N_2/He$ flames

Hao-Yu Hsieh [a], Shenqyang (Steven) Shy [a], Andrei N. Lipatnikov [b,*]

[a] Department of Mechanical Engineering, National Central University, Taoyuan City, 320317, Taiwan
[b] Department of Mechanical Engineering, Chalmers University of Technology, Gothenburg, 412 96, Sweden

ARTICLE INFO

Keywords:
Cellular instability
Expanding spherical flames
Critical Peclet number
Laminar flame speed

ABSTRACT

Experiments with confined spherical laminar flames expanding in lean (the equivalence ratio $\phi = 0.45$) $H_2/O_2/N_2$/He mixtures under room conditions are performed using high-speed Schlieren technique. Measured dependencies of (i) flame radius on time and (ii) flame speed on flame stretch rate are analyzed using four state-of-the-art methods. The following results are worth emphasizing. First, at large ratios of mole fractions X_{He} and X_{N2} of He and N_2, respectively, e.g., $X_{He}/X_{N2} = 1.81$, no visible cellularity was observed within the investigated flame radius range. Second, experimental data obtained at $X_{He}/X_{N2} = 0.51$ or 0.45 indicate that both (i) cells on flame surface and (ii) an increase in the flame speed due to flame instability appear at sufficiently large flame radii, more than 7 ms after the end of the spark discharge. This experimental finding is consistent with the standpoint that high stretch rates can suppress diffusional-thermal and Darrieus-Landau instabilities. Third, the performed measurements demonstrate that changing He:N_2 ratio in lean $H_2/O_2/N_2$/He mixtures offers the opportunity to explore onset of cellular instability by separating it from ignition stage. Fourth, the experiments also show that although the truncation of the data obtained at large flame radii offers the opportunity to explore apparently stable flames in the case of a negative Markstein number Ma_b, such a method results in fitting-dependent and scattered values of laminar flame speeds and, especially, Ma_b.

Novelty and significance statement

New experimental data obtained from expanding spherical laminar lean $H_2/O_2/N_2$/He flames show that both cells on flame surface and an increase in the flame speed due to flame instability may appear at sufficiently large flame radii, well after spark ignition. These results are consistent with the standpoint that high stretch rates suppress diffusional-thermal and Darrieus-Landau instabilities. The performed measurements demonstrate that changing He:N_2 ratio in lean $H_2/O_2/N_2$/He mixtures offers the opportunity to explore onset and development of cellular instability of expanding spherical laminar flames by separating this onset from ignition stage. The obtained results are of importance for modelling turbulent burning of lean hydrogen, specifically, for modelling interactions between turbulent stretch rates and local flame instabilities. The newly introduced method (gradual variations of a ratio of helium and nitrogen mole fractions in lean $H_2/O_2/N_2$/He mixtures) opens new perspectives for experimental research into cellular instability of laminar flames.

1. Introduction

Rapidly growing interest in the utilization of energy bonded in carbon-free fuels such as hydrogen [1] greatly promotes research into diffusional-thermal instability of lean H_2-air laminar flames [2]. As reviewed elsewhere [3], a series of Direct Numerical Simulation (DNS) studies of such flames were performed by several research groups over the past decade. While these studies thoroughly explored diffusional-thermal instability of initially planar laminar flames under various conditions, growth of a curved flame kernel in an initially quiescent lean H_2-air mixture has received less attention despite curvature of a flame kernel is well known to greatly affect another, hydrodynamic or Darrieus-Landau (DL), flame instability [4].

Specifically, sufficiently high rates of stretching of a spherical flame of a finite thickness (in conjunction with molecular transfer within the flame) can suppress DL instability [5–7]. Peclet numbers $Pe = R_f/\delta_L$

* Corresponding author.
E-mail addresses: lipatn@chalmers.se, lanna616800@gmail.com (A.N. Lipatnikov).

https://doi.org/10.1016/j.combustflame.2026.115441
Received 22 June 2026; Received in revised form 28 October 2026; Accepted 28 October 2026
Available online 4 November 2026
0010-2180/© 2026 The Authors. Published by Elsevier Inc. on behalf of The Combustion Institute. This is an open access article under the CC BY license (http://creativecommons.org/licenses/by/4.0/).

associated with onset of DL instability of spherically expanding flames were measured by many research groups [8–10] under various conditions. Here, R_f and δ_L are flame radius and flame thickness, respectively. Transition from stable (small *Pe*) to unstable (large *Pe*) regimes of spherical laminar flame propagation was also predicted theoretically under an assumption of $Pe \gg 1$ [5,7]. However, this result holds only if Lewis number $Le = D/a$ is larger than a critical value Le_{cr}, which is smaller than unity [5]. Here, a is molecular heat diffusivity of a mixture and D is molecular diffusivity of deficient reactant in that mixture. If $Le < Le_{cr} < 1$, the theory implies that "the expanding flame becomes cellular during the initial phase of propagation, i.e., when its radius is comparable to its thickness" [5, p. 78].

Thus, for lean H_2-containing mixtures susceptible to diffusional-thermal instability, onset of the unstable stage of laminar spherical flame expansion remains to be explored. The present authors are aware of two papers [11,12] where laminar flame radius "for onset of instability" is reported for a mixture, which could be susceptible to diffusional-thermal instability, i.e., lean (the equivalence ratio $\phi = 0.6$) H_2-air mixture at room temperature and pressures up to 5 atm. However, in line with the theory [5], the reported radii are small, e.g., smaller than 6.5 mm at 5 atm [11, Fig. 14] or smaller than 10 mm at 2 atm [12, Fig. 4a]. Since so-small flame radii are often associated with the substantial influence of spark ignition on the flame kernel growth [13–20], the experimental data reported in Refs [11,12] do not warrant separation of ignition and unstable stages of flame propagation. Accordingly, the conditions investigated in the cited papers do not seem to allow a target-directed study of onset of diffusional-thermal instability of lean H_2-air spherical flames.

Moreover, to the best of the present authors' knowledge, capability of high stretch rates to stabilize expanding spherical flames susceptible to diffusional-thermal instability has not yet been investigated experimentally despite this issue is of importance for modeling lean burning of H_2-containing mixtures in turbulent flows [21–23].

Accordingly, the present work aims to contribute to bridging these gaps in fundamental knowledge by experimentally exploring onset of cellular instability of spherical flame kernels expanding in initially quiescent lean $H_2/O_2/N_2$/He mixtures susceptible to both diffusional-thermal and DL instabilities.

The key idea of this study stems from experiments [24–26], which have shown that substitution of N_2 with He in lean H_2-air mixtures offers the opportunity to stabilize sufficiently large flame kernels even under elevated pressures. In such experiments, diffusional-thermal instability is weakened, because substitution of N_2 with He results in significantly increasing heat diffusivity of the mixture and shifting Lewis number to unity. Thus, (i) while diffusional-thermal instability of a low-*Le* lean H_2-air expanding spherical laminar flame appears quite early (almost after spark ignition [11,12]), which makes it difficult to separate ignition and unstable stages, (ii) that instability (not DL one!) is suppressed when N_2 is fully substituted with sufficiently large amount of He [26]. Accordingly, the use of an intermediate mixture composition (a part of N_2 is substituted with moderate amount of He) is expected to allow us to substantially delay onset of cellular instability of an expanding spherical flame. Therefore, transition between stable and unstable stages of flame-kernel growth could be separated from the ignition stage, thus enabling study of that transition. This new idea, which was not considered in earlier studies [24–26], is implemented in experiments discussed in the next section.

2. Experimental setup

Since the present measurements closely followed the previous work [26], we shall restrict ourselves to a summary and refer the interested reader to the cited paper.

Centrally ignited, expanding lean $H_2/O_2/N_2$/He laminar spherical flames were experimentally studied using a constant-pressure, constant-temperature, dual-chamber cruciform burner. The burner and associated diagnostics are detailed in Ref [27].

Time evolutions of flame kernels ignited by a spark were recorded using Schlieren technique by a CMOS high-speed camera (Phantom 711) operated at 10,000 frames/s with 800 × 800 pixels. Each flame image was processed adopting the Canny Edge Detection method to obtain an area $A(t)$ enveloped by the flame, whose mean radius was evaluated as follows: $\langle R_f \rangle(t) = [A(t)/\pi]^{1/2}$. Uncertainty in finding the flame radius is estimated to be one pixel, i.e., about 0.16 mm [26]. The measurements were restricted to $\langle R_f \rangle(t) < 46$ mm. Thus, the measured flame radius was always smaller than 1/3 radius of the chamber to satisfy a widely accepted criterion [28] of spherical flame propagation in a cylindrical confinement. For each mixture composition, five runs were performed.

The recorded $\langle R_f \rangle(t)$-curves were fitted adopting four widely used methods [20,29,30]: (i) LS, i.e., linear with respect to flame stretch rate $\dot{s} = (2/\langle R_f \rangle) d\langle R_f \rangle/dt$ [31], (ii) LC, i.e., linear with respect to flame curvature $2/\langle R_f \rangle$ [32], (iii) non-linear NL1 [33], and (iv) non-linear NL2 [34], see Eqs. (3), (5), (8), and (10), respectively, in Ref [26].

When fitting the measured $\langle R_f \rangle(t)$-curves, data obtained at $\langle R_f \rangle(t) < R_i^* = 10$ mm were not analyzed to avoid the ignition influence in the early stage of laminar flame development. Although the flame radius R_i associated with transition from ignition to flame-propagation stage depends on temperature, pressure, mixture characteristics, and parameters of the ignition system [35], such effects are disregarded and a large value of $R_i^* = 10$ mm is set. As will be discussed in Sec. 3.2, this limitation does not alter the major conclusions regarding the four fitting methods.

Major characteristics of studied mixtures are listed in Table 1, where S_L^0 and $\delta_L = (T_b - T_u)/\max\{dT/dx\}$ are the flame speed and thickness, respectively, and $\sigma = \rho_u/\rho_b$ is the density ratio. These characteristics of unstretched laminar flames have been computed using a chemical mechanism by Burke et al [36], the multi-component transport model including Soret effect, and software Chemkin-2 [37,38] under room conditions. In all cases, the equivalence ratio $\phi = 0.45$. In the next-to-the-right column,

$$\frac{\omega_{DL}}{kS_L^0} = \frac{\sqrt{\sigma^3 + \sigma^2 - \sigma} - \sigma}{1 + \sigma} \tag{1}$$

is the normalized growth rate of DL instability for a perturbation with wave number k [4].

The mixtures have been selected as follows. First, based on our recent experimental results [26], a mixture of $0.9H_2+O_2+8.88$He was set to be a starting point. As discussed in detail in the cited paper, such flames were stable in those measurements.

Second, at each subsequent step, the ratio X_{He}/X_{O2} of the mole fractions of He and O_2, respectively, was decreased by a factor of two and X_{N2} was increased to retain the same computed S_L^0. These steps were taken until cellular instability of the studied flame became apparent.

Finally, based on the two latest sets (2.22He and 1.11He), two extra intermediate sets of 1.66He and 1.86He were designed by varying X_{He}/X_{O2}.

Table 1
Major characteristics of studied mixtures.

Mixture composition in moles	S_L^0, m/s	δ_L, mm	σ	$\frac{\omega_{DL}}{kS_L^0}$	*Le*
$0.9H_2+O_2+8.88$He	0.19*	1.82	3.89	0.92	0.92
$0.9H_2+O_2+4.44$He$+2.45N_2$	0.19	1.39	4.04	0.95	0.86
$0.9H_2+O_2+2.22$He$+3.475N_2$	0.19	1.03	4.18	0.99	0.60
$0.9H_2+O_2+1.86$He$+3.64N_2$	0.19	0.97	4.21	0.99	0.53
$0.9H_2+O_2+1.66$He$+3.73N_2$	0.19	0.94	4.24	1.00	0.51
$0.9H_2+O_2+1.11$He$+3.95N_2$	0.19	0.86	4.28	1.01	0.43

*Measured in Ref [26].

3. Results and discussion

3.1. Onset of instability

Typical Schlieren images of the laminar flames studied are shown in Fig. 1. In the reference case of 8.88He, the flame surface is smooth and almost symmetrical during the entire measurement period. No visible cellularity is observed within the investigated flame radius range. Other data obtained in this case are discussed in detail in Ref [26].

Images recorded in the case of 4.44He are very similar and do not indicate any cellularity either.

In the case of 2.22He, flame-surface perturbations are observed around spark electrodes when $\langle R_f \rangle(t) > 25$ mm. However, the most part of the flame surface looks smooth even at the largest measured $\langle R_f \rangle = 45.2$ mm. While substitution of N_2 with He can mitigate diffusional-thermal instability, this method does not suppress DL instability [24–26], which is promoted with decreasing Lewis number if $Le > Le_{cr}$ [5–7]. Accordingly, flame-surface perturbations observed in the case of 2.22He cannot be clearly linked to diffusional-thermal instability, while such a link is not excluded. For instance, the perturbations around the electrodes are small-scale, which is typical for diffusional-thermal instability. Nevertheless, for the sake of rigor, conclusions regarding eventual appearance of diffusional-thermal instability in the case of 2.22He will not be drawn.

It is worth stressing that identification of the type of flame instability is an issue, which still requires investigations. For instance, theoretical equations for instability growth rate ω, obtained using activation energy asymptotic analysis of single-step-chemistry flames, e.g., see Ref [39], read

$$\omega = \omega_{DL} + \omega_2 \tag{2}$$

where ω_2 depends on flame structure and involves several terms, including a term proportional to $Ze(1 - Le)$. From the theoretical perspective, diffusional-thermal instability appears if $\omega_2 > 0$ when $Ze(1 - Le)$ is positive and sufficiently large. Due to other (negative) contributions to ω_2, this happens if $Le < Le_{cr} < 1$.

However, the present authors are not aware of a similar criterion, which could be adopted for analyzing experimental data obtained from complex-chemistry flames. Intensification of flame instability with decreasing Le does not prove appearance of diffusional-thermal instability, because ω is increased with decreasing Le even if $\omega_2 < 0$ [39]. Negative value of a Markstein number Ma does not show that either, because theoretical expressions for ω_2 and Ma, derived using the same methods under the same assumptions, e.g., see Refs [39] and [40],

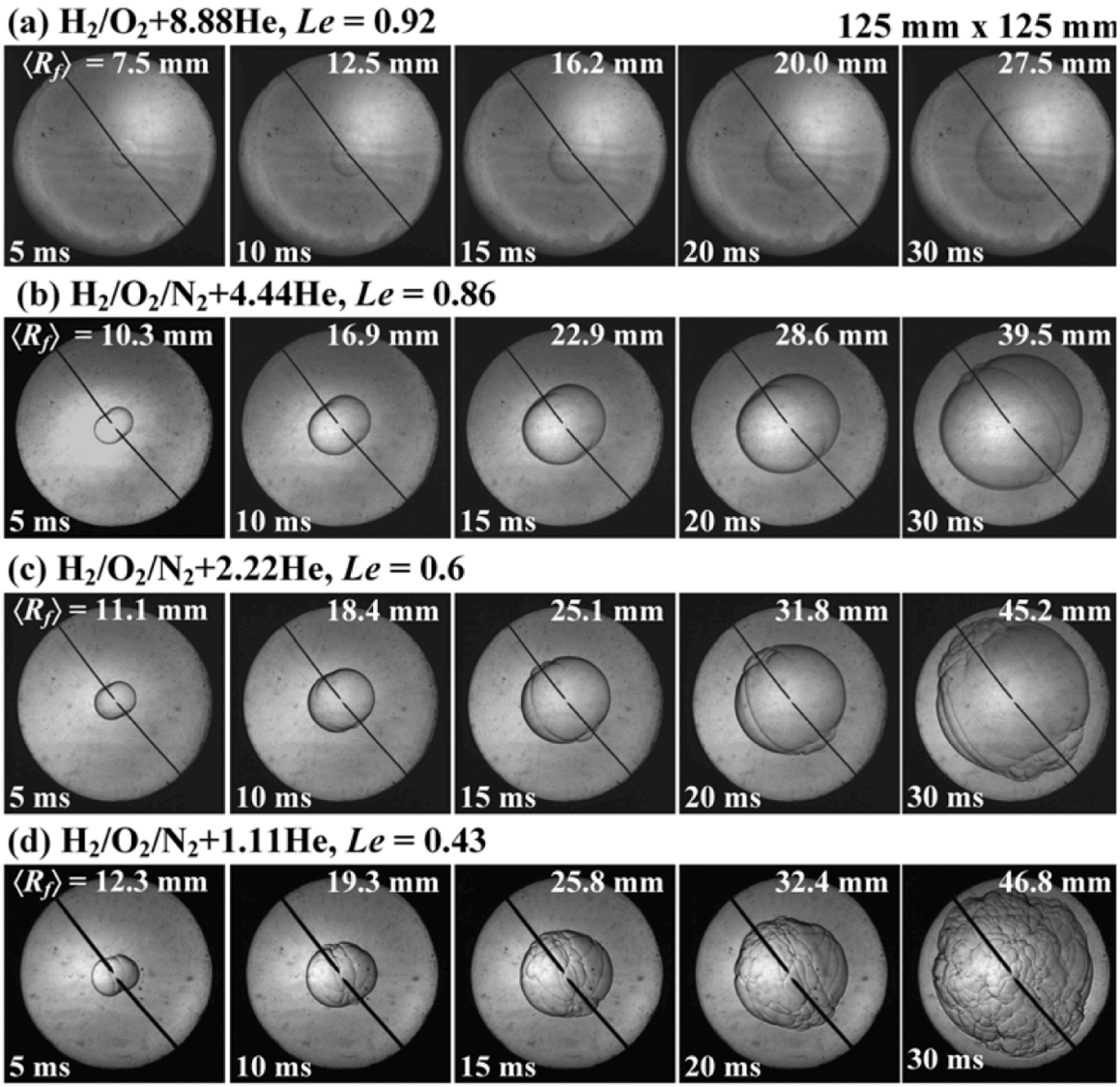

Fig. 1. Typical images of laminar flames in the cases of (a) 8.88He, (b) 4.44He, (c) 2.22He, and (d) 1.11He.

respectively, show that both ω_2 and Ma can be negative in the same flame. In practice, appearance of small-scale cells, see Fig. 1d, is often associated with diffusional-thermal instability, because dispersion curves $\omega(k)$ peak at significantly larger wavenumbers k_m (smaller wavelengths) in the case of diffusional-thermal instability [41], (Fig. 2). However, the present authors are not aware of a study that shows a significant change in k_m under conditions close to appearance of diffusional-thermal instability, i.e., when the sign of ω_2 changes from negative to positive. Therefore, while significantly different (small or large) cell sizes can indicate different (diffusional-thermal or DL, respectively) instabilities under substantially different conditions, such a criterion does not seem to be well elaborated for detecting occurrence of the former instability when experimental conditions are slightly changed to change the sign of ω_2. For the above reasons, a solid conclusion regarding the type of flame instability in the case of 2.22He cannot be drawn, although the images of large flame kernels in Fig. 1c are better associated with DL instability.

In the case of 1.11He, small-scale cells associated with diffusional-thermal instability are well observed.

In the cases of 1.86 He and 1.66He, such small-scale cells are well observed for all five runs in Figs. 2 and 3, respectively, but the cells appear when the flame kernel is sufficiently large. Images presented in the middle column are associated with appearance of such cells and point to onset of cellular instability.

At these instants, the radii $\langle R_f \rangle$ vary from 22 to 25.7 mm in case 1.86He or from 18.9 to 21 mm in case 1.66He, thus implying sufficient separation from the ignition stage. Peclet numbers $Pe = \langle R_f \rangle / \delta_L$ vary from 23 to 26 or from 20 to 22 and are much smaller than critical Peclet numbers reported in the case of DL instability of flames characterized by $Le > Le_{cr}$, e.g., 350 [8], 1000 [9], or 1660 [10]. So large differences between critical Peclet numbers obtained in the present experiments and in earlier studies of DL instability of spherical laminar flames [8–10] indicate that it is diffusional-thermal instability that controls cell formation in present measurements.

Moreover, comparison of Figs. 1c, 2, and 3 shows that small-scale cells are hardly visible at t=20 ms in case 2.22He, but are well observed at $10.4 \leq t_{cr} \leq 12.8$ ms and $8.2 \leq t_{cr} \leq 9.4$ ms in cases 1.86He and 1.66He, respectively. Here, t is time counted from spark ignition and reported in the left bottom corner in each image; subscript cr refers to critical conditions (onset of cellularity). Since the three mixtures are characterized by almost equal δ_L and almost equal ω_{DL}/kS_L^0, see Table 1, such significant differences in the duration t_{cr} of the time intervals required for the appearance of cells on flame surfaces can hardly be explained by DL instability. These differences are better associated with

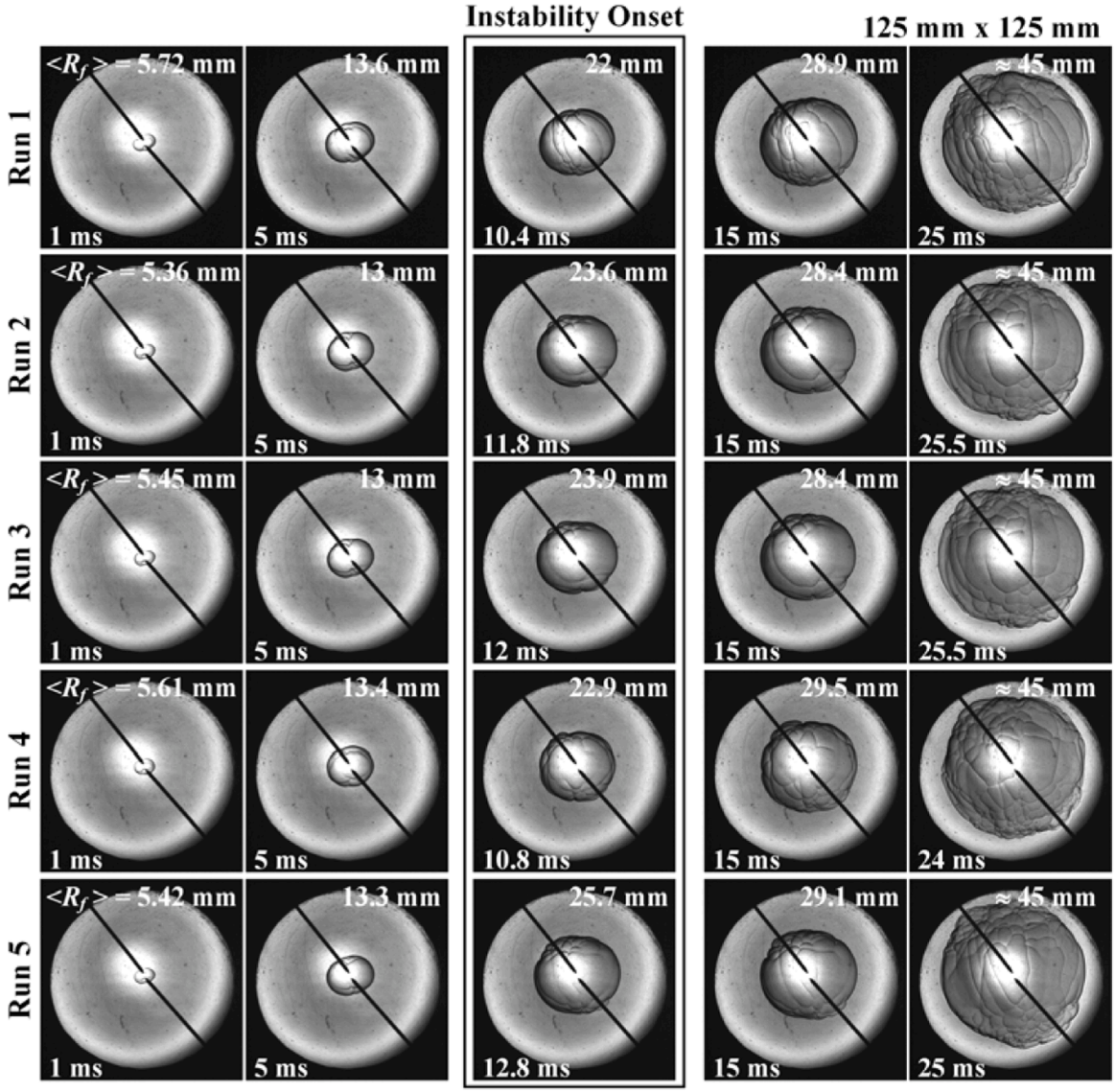

Fig. 2. Images of five laminar flames in case 1.86He.

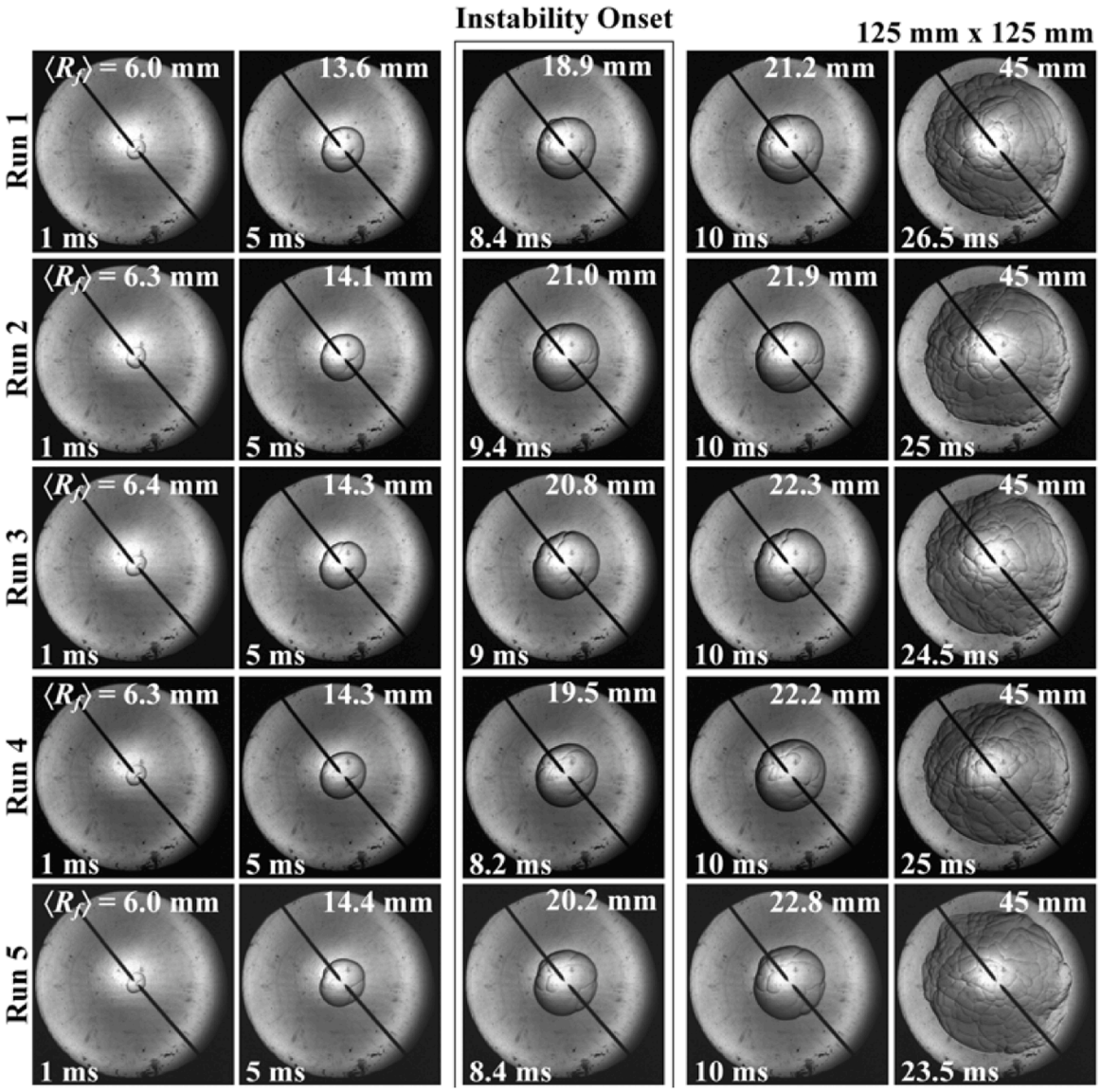

Fig. 3. Images of five laminar flames in case 1.66He.

diffusional-thermal instability.

The facts that the transition from the stable stage to the unstable stage (i) is observed at moderately large $\langle R_f \rangle$ or $Pe \geq 20$ and (ii) is well separated from the ignition stage are consistent with the standpoint that large stretch rates affecting the flames at smaller $\langle R_f \rangle$ suppress diffusional-thermal instability. Such an interpretation is also supported by the facts that (i) contribution of strain rate to the rate of stretching of an expanding spherical laminar flame is larger than curvature contribution by a factor of $(\sigma - 1)$ [40] and (ii) suppression of flame instabilities by high strain rates was theoretically predicted [42–44] and

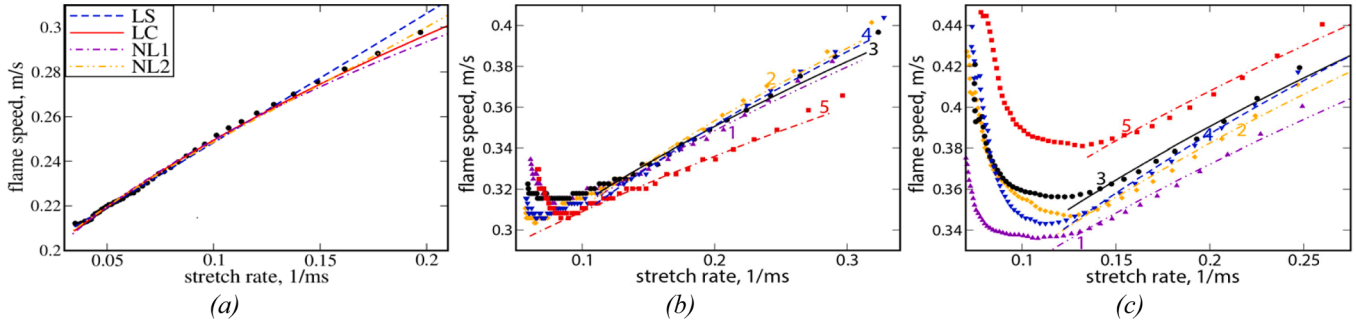

Fig. 4. Flame speeds $\sigma^{-1} d\langle R_f \rangle / dt$ *vs.* stretch rates $\dot{s}$, measured (symbols) in (a) a single representative run in the case of 4.44He or in all five runs in the cases of (b) 2.22He and (c) 1.66He. Curves fit the data using (a) either all four adopted methods at $\langle R_f \rangle > 10$ mm or (b)-(c) LC method at 10 mm $< \langle R_f \rangle <$ 25 mm. (b)-(c) Shown near curves are run numbers.

was observed in recent numerical studies of lean H_2-air flames [45,46]. However, stretch rate evaluated at $t = t_{cr}$ is likely to be smaller than stretch rate required to stabilize the flame, as will be discussed later.

Fig. 4a shows typical results of fitting single-run data (symbols) on $S_L = \sigma^{-1} d\langle R_f \rangle / dt$ vs. $\dot{s} = (2/\langle R_f \rangle) d\langle R_f \rangle / dt$, obtained using different methods (lines). These fitting methods and results are further discussed in the next subsection. Here, it is worth emphasizing different shapes of the $S_L(\dot{s})$-curves. In all three cases addressed in Figs. 4a, 4b, and 4c (since results obtained from flames 1.86He and 1.66He are similar, the former results are not shown for brevity), S_L is decreased with decreasing $\dot{s}$ at large stretch rates (small $\langle R_f \rangle$). This trend stems from a decrease in the strength of diffusional-thermal effects, which result in increasing S_L^0 in lean mixtures that contain H_2 [2,31,39,40].

In case 4.44He, the decreasing $S_L(\dot{s})$ is observed at all stretch rates. In two other cases, see symbols in Figs. 4b and 4c, the trend reverses and S_L increases with decreasing stretch rate (increasing $\langle R_f \rangle$ or Pe) at certain $\dot{s}_{cr}$. This change of the sign of $dS_L/d\dot{s}$ is associated with the influence of flame instability on S_L. In line with Figs. 1c and 3, such a transition occurs at lower $\dot{s}$ (larger $\langle R_f \rangle$) in flames 2.22He, cf. minimum points in Figs. 4b and 4.

Figs. 3 and 4 show that both flame radii $\langle R_f \rangle_{cr}^{*}$ associated with appearance of cellular flames and flame radii $\langle R_f \rangle_{cr}^{**}$ linked with the minimum S_L are scattered from run to run. This scatter could be attributed to the influence of perturbations created by the spark (memory effect). In case 2.22He, $\langle R_f \rangle_{cr}^{**}$ varies from 30.5 to 39.8 mm, its mean and rms values are equal to 36.5 and 4 mm, respectively. In case 1.66He, the counterpart numbers are 23.4, 26.2, 24.9, and 1 mm, respectively. Stretch rates $\dot{s}_{cr}$ associated with the change of sign of $dS_L/d\dot{s}$ from negative to positive are equal to 0.072 ± 0.008 and 0.120 ± 0.009 ms^{-1} in cases 2.22He and 1.66He, respectively.

The reported values of the critical flame radii show that $\langle R_f \rangle_{cr}^{**}$ is substantially larger than $\langle R_f \rangle_{cr}^{*}$, e.g., $\langle R_f \rangle_{cr}^{**} \geq 23.4$ mm, whereas $\langle R_f \rangle_{cr}^{*} \leq 21$ mm in case 1.66He. This difference in $\langle R_f \rangle_{cr}^{*}$ and $\langle R_f \rangle_{cr}^{**}$ may be attributed to the growth of $\langle R_f \rangle(t)$. Indeed, for perturbation to substantially change flame speed, the perturbation magnitude should grow significantly faster than the flame radius [2].

The smaller radii $\langle R_f \rangle_{cr}^{*}$ do not characterize appearance of instability either, as the influence of stretching of an expanding flame on its instability is subject to transient effects. For instance, such effects involve (i) competition between an increase in flame surface area due to instabilities and growth of the flame itself or (ii) an increase in the instability growth rate $\omega(k)$ due to expansion of an interval of perturbation wavenumbers k that can affect the growing flame kernel [46].

3.2. Flame speeds and Markstein lengths

Since partial substitution of N_2 with He offers the opportunity to separate the ignition stage from the cellular stage of laminar flame kernel growth, a part of the measured data on $\langle R_f \rangle$ may be associated with highly stretched stable laminar flames, i.e., flames with smooth surfaces. Accordingly, this part of the data was adopted to asses four different methods (LS, LC, NL1, and NL2) used widely to evaluate unperturbed laminar flame speeds S_L^0 and Markstein lengths L_b by processing measured $\langle R_f \rangle(t)$-curves. When compared to numerous previous experimental studies, the peculiarity of the present analysis consists in exploring highly curved flames characterized by low Lewis numbers.

Different lines in Fig. 4a show that all methods yield close results in case 4.44He. This observation is supported by the values of S_L^0, averaged over five runs and listed in Table 2. These values are close to $S_L^0 = 0.19$ m/s computed using a mechanism by Burke et al [36] or measured in the case of 8.88He [26]. The fitted values of Markstein number $Ma_b = L_b/\delta_L$, yielded by those methods, are more scattered and negative, indicating importance of diffusional-thermal effects. Thus, all four methods perform reasonably well in case 4.44He. If performance of a method is characterized by the rms scatter of the values of Ma_b (the rms scatter of the values of S_L^0 are comparable in all four cases), the LS method could be prioritized, but much more data are required to explore this observation.

Curves plotted in lines in Figs. 4b and 4c fit the measured data (symbols) on $S_L(\dot{s})$ using LC method in a range of 10 mm $< \langle R_f \rangle <$ 25 mm. This interval of flame radii is bounded by 25 mm to reduce the influence of flame instability on its speed. Curves calculated using other methods in the same range of $\langle R_f \rangle$ look similar and are not plotted to make the figures readable.

Although the measured $S_L(\dot{s})$-curves are well fitted (if the range of the analyzed flame radii is bounded by $\langle R_f \rangle = 25$ mm) in cases 2.22He and 1.66He, the fitted flame speeds or Markstein numbers, listed in Table 2, are more scattered when compared to case 4.44He. This scatter casts doubts on the capabilities of each method, because none of them has gained universal recognition as superior to the others.

Another issue with these methods is illustrated in Fig. 5, which shows values of S_L^0, obtained by processing experimental data within an interval of the flame radii, i.e., $R_i^* < \langle R_f \rangle(t) < R_f^{max}$, where $R_i^* = 10$ mm. When R_f^{max} is decreased, S_L^0 is weakly varied in case 4.44He but is significantly decreased in case 2.22He and, especially, 1.66He. At $R_f^{max} < 30$ mm ($\Delta R_f = R_f^{max} - R_i^* < 20$ mm), both (i) differences in S_L^0 yielded by different methods and (ii) the sensitivity $dS_L^0/d\Delta R_f$ of S_L^0 to ΔR_f are significantly increased with decreasing ΔR_f, thus indicating poor performance of these methods for highly stretched flames 2.22He and 1.66He, where diffusional-thermal effects are well pronounced.

Since, in cases 2.22He and 1.66He, the fitted S_L^0 decreases with decreasing R_f^{max}, Fig. 5 indicates that processing $\langle R_f \rangle(t)$-curves, measured in a narrow range of flame radii in the case of $Ma_b < 0$, results in overestimating and fitting-dependent S_L^0 even if cellular instability is not observed in this narrow range of small $\langle R_f \rangle(t)$. These experimental results validate (for the first time to the best of the authors' knowledge) earlier results by Wu et al [29], obtained in one-dimensional simulations.

Issues with the tested methods (i.e., significant differences in the values of S_L^0 or Ma_b, yielded by different methods, or large sensitivities

Table 2
Fitting parameters.

Case		4.44He	2.22He	1.86He			1.66He		
interval $\langle R_f \rangle$, mm		(10,45)	(10,25)	(10,25)	(10,18)	(15,20)	(10,25)	(10,18)	(15,20)
LS	S_L^0, m/s	0.190 ± 0.004	0.277 ± 0.005	0.30 ± 0.01	0.30 ± 0.01	0.31 ± 0.01	0.29 ± 0.01	0.31 ± 0.01	0.28 ± 0.01
	Ma_b	-2.32 ± 0.02	-1.4 ± 0.2	-1.7 ± 0.2	-1.9 ± 0.2	-1.7 ± 0.2	-2.4 ± 0.2	-1.9 ± 0.1	-2.4 ± 0.1
LC	S_L^0, m/s	0.179 ± 0.003	0.263 ± 0.009	0.29 ± 0.01	0.25 ± 0.02	0.29 ± 0.01	0.26 ± 0.02	0.28 ± 0.02	0.25 ± 0.02
	Ma_b	-3.88 ± 0.09	-2.3 ± 0.5	-2.9 ± 0.5	-4.3 ± 0.9	-2.6 ± 0.4	-5.0 ± 0.7	-4.0 ± 0.5	-4.8 ± 0.7
NL1	S_L^0, m/s	0.173 ± 0.003	0.25 ± 0.01	0.27 ± 0.02	0.23 ± 0.2	0.28 ± 0.02	0.23 ± 0.02	0.26 ± 0.02	0.23 ± 0.02
	Ma_b	-5.2 ± 0.2	-3.2 ± 0.9	-4 ± 1	-7 ± 2	-3.6 ± 0.6	-8 ± 2	-6 ± 1	-8 ± 1
NL2	S_L^0, m/s	0.181 ± 0.004	0.263 ± 0.009	0.29 ± 0.01	0.27 ± 0.01	0.29 ± 0.01	0.27 ± 0.01	0.30 ± 0.01	0.26 ± 0.01
	Ma_b	-3.71 ± 0.06	-2.3 ± 0.05	-2.9 ± 0.4	-3.4 ± 0.3	7 ± 2	-4.2 ± 0.3	-3.3 ± 0.2	-4.3 ± 0.3

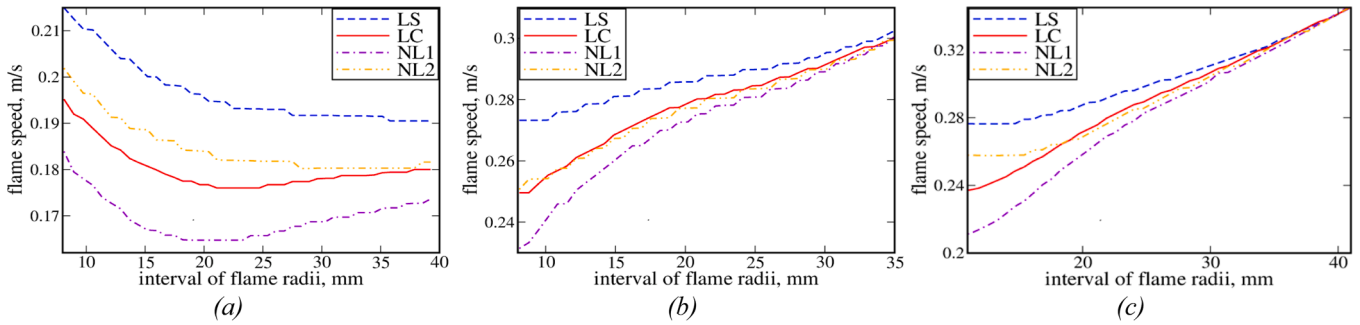

Fig. 5. Values S_L^0 of laminar flame speeds yielded by different methods applied to processing experimental data within various intervals $\Delta R_f = R_f^{max} - R_i^*$ of flame radii. (a) 4.44He, (b) 2.22He and (c) 1.66He.

$dS_L^0/d\Delta R_f$ and $dMa_b/d\Delta R_f$) are also demonstrated for Markstein numbers in Fig. 6 and for both S_L^0 and Ma_b in Table 2, where results obtained by processing the same data on $\langle R_f \rangle(t)$ within three different intervals of flame radii, i.e., 10 mm< $\langle R_f \rangle(t)$ <25 mm, 10 mm< $\langle R_f \rangle(t)$ <18 mm, and 15 mm< $\langle R_f \rangle(t)$ <20 mm, are reported in cases 1.86He and 1.66He. Note that methods LC and NL2 yield close results in all cases, because differences between them are of the second order with respect to a small perturbation parameter, i.e., normalized curvature δ_L/R_f [34].

The issues emphasized above will not disappear if dependence of the boundary R_i^* of ignition stage on mixture composition, pressure, temperature, and parameters of the ignition system is allowed for. On the contrary, since (i) a large value of $R_i^* = 10$ mm is set here and (ii) the differences between the tested methods are larger at larger flame curvature, an analysis of data obtained at $R_i < \langle R_f \rangle(t) < 10$ mm is not expected to reconcile these methods. In other words, such an analysis will not alter the major conclusion; in all likelihood, it will only reinforce it.

One trend observed in Figs. 5 and 6 appears to be surprising at first glance. These figures show that differences between the fitted values of S_L^0 or Ma_b, yielded by different methods, are small when the interval of analyzed flame radii is not restricted and the data obtained from unstable flames are also processed. This trend is explained in Fig. 7, which shows that the fitting $S_L(\dot{s})$-curves, yielded by different methods for the entire interval of $\langle R_f \rangle(t) > 10$ mm, are very close to one another, see color lines, but are very different from the experimental data obtained from the unstable flames. Thus, differences between the $S_L(\dot{s})$-curves obtained from unstable laminar flames (see circles in Fig. 7) and the $S_L(\dot{s})$-curves yielded by the methods studied are so large that small differences between different methods do not play a role. This example shows that close values of S_L^0 (or Ma_b), yielded by different methods, do not prove that these methods perform well.

3.3. Assessment of a recent criterion

The present experimental data offer the opportunity to directly assess the applicability of the following recently proposed scaling parameter [47]

$$\mathscr{P} = Ze/Pe_{\mathrm{CD}} \tag{3}$$

to characterizing the strength of diffusional-thermal effects under conditions significantly different from conditions explored by Rieth et al [47]. Here, Ze is Zeldovich number and the convection-diffusion Peclet number Pe_{CD} is defined

$$Pe_{\mathrm{CD}} = \frac{\left| u \frac{\partial Y_{\mathrm{H_2}}}{\partial x} \right|_{\mathrm{1D,max}}}{\left| \frac{1}{\rho} \frac{\partial}{\partial x} \left(\rho \frac{W_{\mathrm{H_2}}}{W_m} D_{\mathrm{H_2}} \frac{\partial X_{\mathrm{H_2}}}{\partial x} \right) \right|_{\mathrm{1D,max}}} \tag{4}$$

using the maximum values of convection and diffusion fluxes in the unstretched one-dimensional (1D) laminar flame. Here, x and u are axial coordinate and flow velocity, respectively; ρ is the density; $W_{\mathrm{H_2}}$ and W_m are molecular weights of hydrogen and mixture, respectively; $D_{\mathrm{H_2}}$ is diffusivity of H_2; $X_{\mathrm{H_2}}$ and $Y_{\mathrm{H_2}}$ are its mole and mass fractions, respectively.

Table 3 reports Pe_{CD}, Ze, and $\mathscr{P}$ obtained in simulations of the unstretched 1D laminar flames using a chemical mechanism by Burke et al [36], the multi-component transport model including Soret effect, and software Chemkin-2 [37,38]. The Zeldovich numbers have been found by simulating flames where a small amount of inert diluent is substituted with Ar, as described elsewhere [48]. In all cases, the values of $\mathscr{P}$ are approximately equal despite cellular instability manifests itself very differently in the flames studied. Thus, the present experimental data and Table 3 do not support the $\mathscr{P}$ -criterion for $H_2/O_2/N_2$/He mixtures, unlike the DNS data [47] obtained from lean hydrogen-air flames at

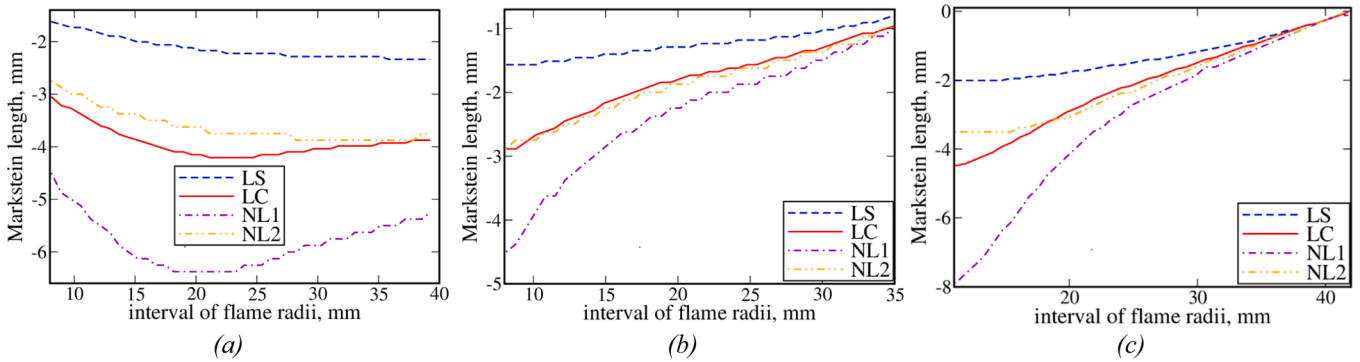

Fig. 6. Values Ma_b of Markstein numbers yielded by different methods applied to processing experimental data within various intervals $\Delta R_f = R_f^{max} - R_i^*$ of flame radii. (a) 4.44He, (b) 2.22He and (c) 1.66He.

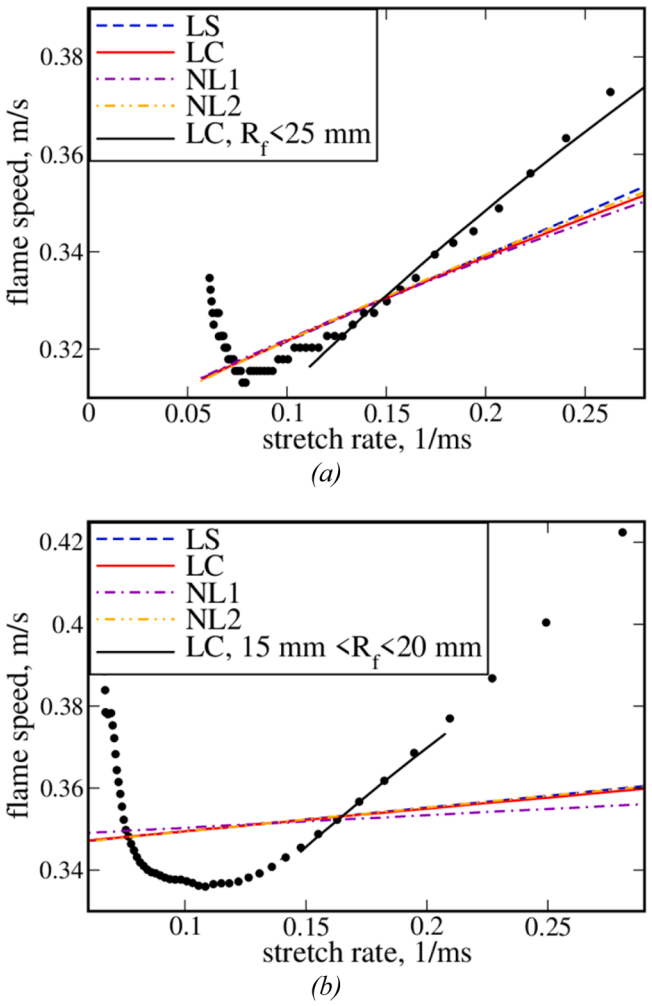

Fig. 7. Examples of processing data (symbols) measured at $\langle R_f \rangle > 10$ mm using four different methods (color lines) specified in legends. Black solid lines show results of LC-processing the same data limited to $\langle R_f \rangle < 25$ mm. (a) 2.22He, (b) 1.66He.

Table 3
Other characteristics of studied mixtures.

Mixture composition	Pe_{CD}	Ze	$\mathscr{P}$	$Ze(1-Le)$
$0.9H_2+O_2+8.88He$	0.24	21.7	90	1.74
$0.9H_2+O_2+4.44He+2.45N_2$	0.18	17.0	94	2.38
$0.9H_2+O_2+2.22He+3.475N_2$	0.16	14.8	93	5.92
$0.9H_2+O_2+1.86He+3.64N_2$	0.16	14.5	94	6.82
$0.9H_2+O_2+1.66He+3.73N_2$	0.15	14.4	94	7.06
$0.9H_2+O_2+1.11He+3.95N_2$	0.15	13.9	94	7.92

various pressures. On the contrary, the values of $Ze(1-Le)$ reported in Table 3 are higher in flames where cellular instability is observed earlier and this trend is completely in line with theories of unstable laminar flames, e.g., see Ref [39].

4. Conclusions

Experimental data obtained in cases 1.86He and 1.66He indicate that cellular instability appears at a sufficiently large flame radius more than 7 ms after the end of the spark discharge, when the ignition effects are expected to be weak. These results demonstrate that changing He:N_2 ratio in lean $H_2/O_2/N_2$/He mixtures offers the opportunity to explore onset of cellular instability by separating it from ignition stage. Moreover, the data are consistent with the standpoint that high stretch rates can suppress both DL and diffusional-thermal instabilities.

The experiments also show that although the truncation of the data measured at large $\langle R_f \rangle(t)$ offers the opportunity to explore apparently stable highly curved flames characterized by negative Ma_b, such a method results in fitting-dependent and widely scattered values of S_L^0 and, especially, Ma_b. Thus, the present experiments validate results obtained earlier by Wu et al [29] in one-dimensional numerical simulations.

CRediT authorship contribution statement

Hao-Yu Hsieh: Writing – review & editing, Visualization, Investigation, Formal analysis, Data curation. **Shenqyang (Steven) Shy:** Writing – review & editing, Writing – original draft, Supervision, Methodology, Investigation, Funding acquisition. **Andrei N. Lipatnikov:** Writing – review & editing, Writing – original draft, Investigation, Formal analysis, Data curation, Conceptualization.

Declaration of competing interest

The authors declare that they have no known competing financial interests or personal relationships that could have appeared to influence the work reported in this paper.

Acknowledgements

SSS acknowledges the financial support by National Science and Technology Council, Taiwan, under grants 114-2221-E-008-036 and 114-2218-E-008-005. ANL acknowledges the financial support by Swedish Research Council (grant 2023-04407).

References

[1] A. Dreizler, H. Pitsch, V. Scherer, C. Schulz, J. Janicka, The role of combustion science and technology in low and zero impact energy transformation processes, Appl. Energy Combust. Sci. 7 (2021) 100040.
[2] Ya.B. Zeldovich, G.I. Barenblatt, V.B. Librovich, G.M. Makhviladze, The Mathematical Theory of Combustion and Explosions, Consultants Bureau, New York, 1985.
[3] H. Pitsch, The transition to sustainable combustion: hydrogen-and carbon-based future fuels and methods for dealing with their challenges, Proc. Combust. Inst. 40 (2024) 105638.
[4] L.D. Landau, E.M. Lifshits, Fluid Mechanics, Pergamon Press, Oxford, 1987.
[5] J.K. Bechtold, M. Matalon, Hydrodynamic and diffusion effects on the stability of spherically expanding flames, Combust. Flame 67 (1987) 77–90.
[6] D. Bradley, Instabilities and flame speeds in large-scale premixed gaseous explosions, Phil. Trans. R. Soc. London 357 (1999) 3567–3581.
[7] R. Addabbo, J.K. Bechtold, M. Matalon, Wrinkling of spherically expanding flames, Proc. Combust. Inst. 29 (2002) 1527–1535.
[8] D. Bradley, C.M. Harper, The development of instabilities in laminar explosion flames, Combust. Flame 99 (1994) 562–572.
[9] C.R. Bauwens, J.M. Bergthorson, S.B. Dorofeev, Experimental study of spherical flame acceleration mechanisms in large-scale propane–air flames, Proc. Combust. Inst. 35 (2015) 2059–2066.
[10] K. Van, A. Hu, J.Z. Fang, T.K. Bera, A.A. Aradi, S.K. Jain, F.N. Egolfopoulos, Quantitative studies of instabilities of confined spherically expanding flames: application to flame propagation and autoignition of natural gas blends with hydrogen at engine-relevant conditions, Combust. Flame 274 (2025) 114009.
[11] G. Jomaas, C.K. Law, J.K. Betchold, On transition to cellularity in expanding spherical flames, J. Fluid Mech. 583 (2007) 1–26.
[12] J. Huo, A. Saha, T. Shu, Z. Ren, C.K. Law, Self-acceleration and global pulsation in expanding laminar H_2-O_2-N_2 flames, Phys. Rev. Fluids 4 (2019) 043201.
[13] T. Tahtouh, F. Halter, C. Mounaïm-Rousselle, Measurement of laminar burning speeds and Markstein lengths using a novel methodology, Combust. Flame 156 (2009) 1735–1743.
[14] F. Halter, T. Tahtouh, C. Mounaïm-Rousselle, Nonlinear effects of stretch on the flame front propagation, Combust. Flame 157 (2010) 1825–1832.
[15] J.X. Zhou, M. Cordier, C. Mounaïm-Rousselle, F. Foucher, Experimental estimate of the laminar burning velocity of iso-octane in oxygen-enriched and CO_2-diluted air, Combust. Flame 158 (2011) 2375–2383.
[16] E. Varea, V. Modica, A. Vandel, B. Renou, Measurement of laminar burning velocity and Markstein length relative to fresh gases using a new postprocessing procedure: application to laminar spherical flames for methane, ethanol and isooctane/air mixtures, Combust. Flame 159 (2012) 577–590.

[17] E. Varea, V. Modica, B. Renou, A.M. Boukhalfa, Pressure effects on laminar burning velocities and Markstein lengths for isooctane-ethanol-air mixtures, Proc. Combust. Inst. 34 (2013) 733–744.
[18] G. Dayma, F. Halter, P. Dagaut, New insights into the peculiar behavior of laminar burning velocities of hydrogen-air flames according to pressure and equivalence ratio, Combust. Flame 161 (2014) 2235–2241.
[19] P. Brequigny, G. Dayma, F. Halter, C. Mounaïm-Rousselle, T. Dubois, P. Dagaut, Laminar burning velocities of premixed nitromethane/air flames: an experimental and kinetic modeling study, Proc. Combust. Inst. 35 (2015) 703–710.
[20] A.N. Lipatnikov, S.S. Shy, W.Y. Li, Experimental assessment of various methods of determination of laminar flame speed in experiments with expanding spherical flames with positive Markstein lengths, Combust. Flame 162 (2015) 2840–2854.
[21] J. Chomiak, A.N. Lipatnikov, Simple criterion of importance of laminar flame instabilities in premixed turbulent combustion of mixtures characterized by low Lewis numbers, Phys. Rev. E 107 (2023) 015102.
[22] H.C. Lee, B. Wu, P. Dai, M. Wan, A.N. Lipatnikov, Turbulent burning velocity and thermodiffusive instability of premixed flames, Phys. Rev. E 108 (2023) 035101.
[23] H.C. Lee, B. Wu, P. Dai, M. Wan, A.N. Lipatnikov, Comparison of characteristics of unstable laminar and turbulent lean hydrogen-air flames, Phys. Fluids 37 (2025) 085182.
[24] S.D. Tse, D.L. Zhu, C.K. Law, Morphology and burning rates of expanding spherical flames in H_2/O_2/inert mixtures up to 60 atmospheres, Proc. Combust. Inst. 28 (2000) 1793–1800.
[25] M.P. Burke, F.L. Dryer, Y. Ju, Assessment of kinetic modeling for lean $H_2/CH_4/O_2$/diluent flames at high pressures, Proc. Combust. Inst. 33 (2011) 905–912.
[26] H.-Y. Hsieh, A.N. Lipatnikov, S.S. Shy, Laminar flame speeds of lean hydrogen-oxygen-helium mixtures under elevated pressures and temperatures, Combust. Flame 281 (2025) 114412.
[27] C.C. Liu, S.S. Shy, H.C. Chen, M.W. Peng, On interaction of centrally-ignited, outwardly-propagating premixed flames with fully-developed isotropic turbulence at elevated pressure, Proc. Combust. Inst. 33 (2011) 1293–1299.
[28] M.P. Burke, Z. Chen, Y. Ju, F.L. Dryer, Effect of cylindrical confinement on the determination of laminar flame speeds using outwardly propagating flames, Combust. Flame 156 (2009) 771–779.
[29] F. Wu, W. Liang, Z. Chen, Y. Ju, C.K. Law, Uncertainty in stretch extrapolation of laminar flame speed from expanding spherical flames, Proc. Combust. Inst. 35 (2015) 663–670.
[30] A.A. Konnov, A. Mohammad, V.R. Kishore, N. Kim, C. Prathap, S. Kumar, A comprehensive review of measurements and data analysis of laminar burning velocities for various fuel+air mixtures, Prog. Energy Combust. Sci. 68 (2018) 197–267.
[31] M.L. Frankel, G.J. Sivashinsky, On effects due to thermal expansion and Lewis number in spherical flame propagation, Combust. Sci. Technol. 31 (1983) 131–138.
[32] V.P. Karpov, A.N. Lipatnikov, P. Wolanskii, Finding the Markstein number using the measurements of expanding spherical laminar flames, Combust. Flame 109 (1997) 436–448.
[33] A.P. Kelley, C.K. Law, Nonlinear effects in the extraction of laminar flame speed from expanding spherical flames, Combust. Flame 156 (2009) 1844–1851.
[34] A.P. Kelley, J.K. Bechtold, C.K. Law, Premixed flame propagation in a confining vessel with weak pressure rise, J. Fluid Mech. 691 (2012) 26–51.
[35] S.S. Shy, Spark ignition transitions in premixed turbulent combustion, Prog. Energy Combust. Sci. 98 (2023) 101099.
[36] M.P. Burke, M. Chaos, Y. Ju, F.L. Dryer, S.J. Klippenstein, Comprehensive H_2/O_2 kinetic model for high-pressure combustion, Int. J. Chem. Kinet. 44 (2012) 444–474.
[37] R.J. Kee, J.F. Crcar, M.D. Smooke, J.A. Miller, PREMIX: A FORTRAN Program for Modeling Steady Laminar One-Dimensional Premixed Flames, Report No. SAND-85-8240, Sandia National Laboratories, 1985.
[38] R.J. Kee, F.M. Rupley, J.A. Miller, CHEMKIN-II: A FORTRAN Chemical Kinetics Package for the Analysis of Gas-Phase Chemical Kinetics, Report No. SAND-89-8009, Sandia National Laboratories, 1989.
[39] M. Matalon, C. Cui, J.K. Bechtold, Hydrodynamic theory of premixed flames: effects of stoichiometry, variable transport coefficients and arbitrary reaction orders, J. Fluid Mech. 487 (2003) 179–210.
[40] G.K. Giannakopoulos, A. Gatzoulis, C.E. Frouzakis, M. Matalon, A.G. Tomboulides, Consistent definitions of "Flame Displacement Speed" and "Markstein Length" for premixed flame propagation, Combust. Flame 162 (2015) 1249–1264.
[41] L. Berger, M. Grinberg, B. Jürgens, P.E. Lapenna, F. Creta, A. Attili, H. Pitsch, Flame fingers and interactions of hydrodynamic and thermodiffusive instabilities in laminar lean hydrogen flames, Proc. Combust. Inst. 39 (2023) 1525–1534.
[42] G.I. Sivashinsky, C.K. Law, G. Joulin, On stability of premixed flames in stagnation-point flow, Combust. Sci. Technol. 28 (1982) 155–159.
[43] G. Joulin, G.I. Sivashinsky, On the linear hydrodynamic stability and response of premixed flames in stagnation-point flows, Symp. (Int.) Combust. 24 (1992) 37–44.
[44] Y. Kortsarts, I. Brailovsky, G.I. Sivashinsky, On hydrodynamic instability of stretched flames, Combust. Sci. Technol. 123 (1997) 207–225.
[45] A. Porcarelli, P.E. Lapenna, F. Creta, I. Langella, Stability analysis of thermodiffusively unstable counterflow lean premixed hydrogen flames, Proc. Combust. Inst. 41 (2025) 105906.
[46] X. Guan, H.C. Lee, T. Zhang, P. Dai, M. Wan, A.N. Lipatnikov, A direct numerical simulation study of stretched laminar lean hydrogen-air flames, Proc. Combust. Inst. 42 (2026) 106394.
[47] M. Rieth, A. Gruber, J.H. Chen, The effect of pressure on lean premixed hydrogen-air flames, Combust. Flame 250 (2023) 112514.
[48] S.M. Mousavi, A.N. Lipatnikov, Dependence of Zel'dovich number on pressure and temperature in lean hydrogen-air mixtures, Proc. Combust. Inst. 40 (2024) 105501.